ELSEVIER

Chemical Geology 169 (2000) 243–262

CHEMICAL GEOLOGY
INCLUDING
ISOTOPE GEOSCIENCE

www.elsevier.com/locate/chemgeo

H_2O diffusion in rhyolitic melts and glasses

Youxue Zhang [a,b,*], Harald Behrens [a]

[a] *Institut für Mineralogie, Universität Hannover, Hanover D-30167, Germany*
[b] *Department of Geological Sciences, University of Michigan, 2534 C.C. Little Building Ann Arbor, MI 48109-1063, USA*

Received 12 April 1999; accepted 13 November 1999

Abstract

H_2O diffusion plays a major role in bubble growth and volcanic eruption. We report a comprehensive study of H_2O diffusion in rhyolitic melts and glasses. This new study and previous investigations together cover a wide range of conditions: 400–1200°C, 0.1–810 MPa, and 0.1–7.7 wt.% total H_2O content (H_2O_t). In order to constrain how the diffusivity depends on H_2O_t, both the diffusion-couple experiments and the dehydration experiments are carried out in a cold-seal vessel (CSV), an internally heated pressure vessel, and a piston cylinder. H_2O concentration profiles are measured by infrared (IR) spectroscopy. Although there are still some experimental and analytical difficulties, our data represent a major improvement over earlier data. The diffusion data have been used to quantify H_2O diffusivity as a function of temperature, pressure, and H_2O_t. Assuming that molecular H_2O (H_2O_m) is the diffusing species, the H_2O_m diffusivity (in $\mu m^2/s$) can be expressed as:

$$D_{H_2O_m} = \exp\left[(14.08 - 13{,}128/T - 2.796P/T) + (-27.21 + 36{,}892/T + 57.23P/T)X\right],$$

where T is in Kelvin, P is in mPa, and X is the mole fraction of H_2O_t on a single oxygen basis. The pressure dependence is not so well-resolved compared to the dependence on T and X. The dependence of $D_{H_2O_m}$ on X increases with increasing pressure. The results are consistent with the data of Nowak and Behrens (1997) [Nowak, M., Behrens, H., 1997. An experimental investigation on diffusion of water in haplogranitic melts. Contrib. Mineral. Petrol. 126, 365–376.], but different from the assumption of Zhang et al. (1991a) [Zhang, Y., Stolper, E.M., Wasserburg, G.J., 1991a. Diffusion of water in rhyolitic glasses. Geochim. Cosmochim. Acta 55, 441–456.], because the dependence cannot be resolved from their low-H_2O_t diffusion data, and because the dependence is not so strong at low pressures. The activation energy for H_2O_m diffusion decreases as H_2O_t increases and depends on P (increases with P at $X < 0.05$ and decreases with P at $X > 0.05$). The results roughly reconcile the different activation energies of Zhang et al. (1991a) and Nowak and Behrens (1997). The total (or bulk) H_2O diffusivity ($D_{H_2O_t}$) can be calculated from $D_{H_2O_t} = D_{H_2O_m} dX_m/dX$, where X_m is the mole fraction of

* Corresponding author. Department of Geological Sciences, University of Michigan, 2534 C.C. Little Building, Ann Arbor, MI 48109-1063, USA.

E-mail address: youxue@umich.edu (Y. Zhang).

PII: S0009-2541(99)00231-4

H_2O_m. This approach can reproduce the $D_{H_2O_t}$ values to within a factor of 2 in the range of 400–1200°C, 0.1–810 MPa, and 0–7.7% H_2O_t. An explicit formula for calculating $D_{H_2O_t}$ at $H_2O_t \le 2\%$ is:

$$D_{H_2O_t} = \frac{C}{C_0}\exp\left(10.49 - \frac{10{,}661}{T} - \frac{1.772P}{T}\right),$$

where C is H_2O_t content by weight, and C_0 equals 1% H_2O_t. A formula for calculating $D_{H_2O_t}$ at all conditions covered by this work is:

$$D_{H_2O_t} = X\exp(m)\left\{1 + \exp\left[56 + m + X\left(-34.1 + \frac{44{,}620}{T} + \frac{57.3P}{T}\right) - \sqrt{X}\left(0.091 + \frac{4.77\times10^6}{T^2}\right)\right]\right\},$$

where $m = -20.79 - 5030/T - 1.4P/T$. The diffusivities obtained in this work can be used to model bubble growth in explosive and nonexplosive rhyolitic volcanic eruptions in all commonly encountered T, P, and H_2O_t conditions.

Keywords: Water diffusion; Rhyolitic melt; Volcanic eruptions; Volatiles; Diffusion coefficients; Speciation

1. Introduction

Diffusion of H_2O in silicate melts and glasses plays a crucial role in bubble growth and silicic volcanic eruptions on terrestrial planets. Shaw (1974) carried out the first study of H_2O diffusion in a rhyolitic melt. He showed that the diffusivity of the H_2O component is high compared to that of other components and increases with its concentration. Subsequent investigations (Friedman and Long, 1976; Jambon, 1979, 1983; Delaney and Karsten, 1981; Karsten et al., 1982; Lapham et al., 1984) confirmed the conclusions. Delaney and Karsten (1981) found from hydration experiments that H_2O diffusion profiles are best modeled by assuming that the diffusivity of the H_2O component increases exponentially with total H_2O concentration. Karsten et al. (1982) showed that the activation energy for total H_2O diffusivity is low. There is also a large literature for H_2O component diffusion in silica and other commercial glasses at very low H_2O concentrations (e.g., Moulson and Roberts, 1961; Doremus, 1995) which will not be reviewed here.

Because dissolved H_2O component is present in silicate melts and glasses as at least two species, H_2O_m molecules, and OH groups, and because H_2O_m and OH are expected to have different diffusivities (for clarity, hereafter, H_2O refers to the H_2O component, H_2O_m refers to molecular H_2O, OH refers to the hydroxyls, and H_2O_t refers to total H_2O content), it is natural to consider the role of speciation in diffusion. Wasserburg (1988) presented a formal analysis on how to treat the diffusion of H_2O component if H_2O_m is the diffusing species. Zhang et al. (1991a) carried out experiments and examined the role of speciation in H_2O diffusion in rhyolitic glass/melt with 0.1–1.8% H_2O_t at 0.1 MPa (1 MPa = 10 bar) and 400–550°C. They treat the one-dimensional diffusion of H_2O component by explicitly considering the role of speciation:

$$\frac{\partial X}{\partial t} = \frac{\partial}{\partial x}\left\{D_{H_2O_m}\frac{\partial X_m}{\partial x} + D_{OH}\frac{\partial X_{OH}/2}{\partial x}\right\}, \qquad (1)$$

where $D_{H_2O_m}$ is the diffusivity of molecular H_2O, D_{OH} is the diffusivity of OH groups, and X, X_m, and X_{OH} are mole fractions of H_2O_t, H_2O_m, and OH on a single oxygen basis (Stolper, 1982; Zhang, 1999). The species concentrations are related to each other by the interconversion reaction:

$$H_2O_m + O \Leftrightarrow 2OH, \qquad (R1)$$

where O is an anhydrous oxygen. From diffusion experiments, H_2O_t, H_2O_m, and OH profiles are measured. Hence, if species concentrations at the experimental temperature are preserved, both $D_{H_2O_m}$ and D_{OH} can be obtained by fitting the measured profiles to the above equation if the diffusivities are assumed to be constant. Whether they are indeed constant can be determined from the quality of the fit. Based on

the dehydration experiments, Zhang et al. (1991a) found that the diffusion coefficient of OH groups is negligible and molecular H_2O is the diffusing species. This result leads to:

$$D_{H_2O_t} = D_{H_2O_m} d X_m / d X, \quad (2)$$

where $D_{H_2O_t}$ is the bulk (or total) H_2O diffusivity. They further inferred that the diffusion coefficient of H_2O_m is almost independent of H_2O_t. The diffusion model of Zhang et al. (1991a) can be successfully applied to calculate the concentration-dependent $D_{H_2O_t}$ for rhyolitic melts at low H_2O_t as long as internal consistency is maintained (Jambon et al., 1992; Zhang, 1999), although later new calibrations of the IR technique (Zhang et al., 1997) imply that $D_{H_2O_m}$ values must be revised. Zhang and Stolper (1991) investigated H_2O diffusion in basaltic melt with 0.04–0.4% H_2O_t at 1000 MPa and 1300–1500°C. They found that $D_{H_2O_t}$ in basaltic melt is significantly higher than that in rhyolitic melt under similar temperatures. Although H_2O_m concentration cannot be directly measured, the observed proportionality between $D_{H_2O_t}$ and H_2O_t led them to suggest that molecular H_2O_m is also the diffusing species. Watson (1994) reviewed the diffusion of water and other volatile components in silicate melts.

Behrens and Nowak (1997) and Nowak and Behrens (1997) conducted H_2O diffusion experiments in a haplogranitic melt and other synthetic melts at higher T (800–1200°C) and 50–500 MPa, to very high H_2O_t (up to 8.5%). They found that the shape of $D_{H_2O_t}$ vs. H_2O_t does not follow that of Zhang et al. (1991a) when H_2O_t content is greater than 2% (especially when it is greater than 3%). Behrens and Nowak (1997) and Nowak and Behrens (1997) found that the dependence of $D_{H_2O_t}$ on H_2O_t is roughly exponential at high H_2O_t, whereas the model of Zhang et al. (1991a) predicts linear or less than linear dependence. Nowak and Behrens (1997) adopted an empirical polynomial equation for the dependence of ln $D_{H_2O_t}$ on H_2O_t content, which can be used for interpolation, but cannot be used at low H_2O_t contents. One purpose of this study is to combine both approaches to understand H_2O diffusion and to describe H_2O diffusivity in a large range of T, P, and H_2O_t space for rhyolitic melt.

Understanding H_2O diffusion in silicate melts is important in two aspects. One is the importance of the data in understanding bubble growth and volcanic eruptions (e.g., Navon et al., 1998; Proussevitch and Sahagian, 1998). The second is that this is a diffusion problem for a multi-species component (Zhang et al., 1991b) with one species more mobile than the other and hence, is theoretically interesting. There are other systems in which mobile and immobile ''species'' are inferred but cannot be directly measured (e.g., Moulson and Roberts, 1961; Doremus, 1995; Cooper et al., 1996; Wang et al., 1996). Therefore, a detailed understanding of the role of H_2O_m and OH in H_2O diffusion, where both can be measured (even with complexities discussed below), may be instructive to these other systems in which mobile and immobile species are not directly measurable.

We report here a comprehensive study of H_2O diffusion in rhyolitic melts and glasses as a function of T, P, and H_2O_t, with emphasis on understanding H_2O diffusion in a large range of H_2O_t content from 0.08 to 7.7 wt.% H_2O_t, and on obtaining an expression for predicting the diffusivity as a function of T, P, and H_2O_t. In most of the diffusion experiments of Nowak and Behrens (1997), the run times probably were too long, and water was lost from the hydrous half of the diffusion couple by diffusion to the surfaces. It is unclear as to which extent this has influenced their derived diffusion data. In our new study, we conduct diffusion runs with high water contents up to 7.7 wt.% using improved experimental techniques. With the improvements, short-duration experiments can be performed with well-controlled thermal history. Thus, the new diffusion data are more reliable for very high water contents than the data of Nowak and Behrens (1997). From the new data, we derive an expression for $D_{H_2O_t}$ that is accurate to within a factor of 2 at 400–1200°C, 0.1–810 MPa, and 0–7.7% H_2O_t, and can be applied to treat H_2O diffusion in bubble growth in rhyolitic systems.

2. Experimental and analytical methods

2.1. Experimental methods

Both natural rhyolitic glasses and experimentally hydrated rhyolitic glasses are used in experiments.

Natural rhyolitic glasses are from Mono Craters and contain 0.1–2.0% H_2O_t. They also contain a small amount of microlites/microphenocrysts and bubbles but the effect of these on the diffusion results is negligible (Zhang et al., 1991a). H_2O_t content in a starting glass may vary by 5% relative, and in one case, varies by 10% relative.

In order to investigate H_2O diffusion at high H_2O_t, some experimentally hydrated rhyolitic glasses are prepared by adding water to natural rhyolitic glasses at high T. To obtain large and homogeneous glass pieces (20 mm in length and 5 mm in diameter), water and glass powder were loaded into gold capsules in turns in several steps. Synthesis was performed in an internally heated pressure vessel at 1000°C and at 500 MPa for 2 days. The experimentally hydrated glass samples are free of crystals and bubbles. Small pieces of 10–20 mg were cut from both ends of each hydrous glass to determine the total H_2O content by pyrolysis and subsequent Karl–Fischer titration (see Behrens et al., 1996 for description of this method). Differences in H_2O_t determined from the two end pieces are always below 5% relative. Mean water contents of the hydrated glasses are 3.8–7.7% as shown in Table 1.

2.1.1. Dehydration experiments

Dehydration experiments were conducted at Universität Hannover in a rapid-quench cold-seal vessel (CSV) except for one experiment (KS-D14, which was conducted at 0.1 MPa and experienced bubble growth). The high pressure is necessary to prevent bubble growth. The heating-up duration was about 30 min and rapid cooling was accomplished by turning the furnace upside down so that the sample drops to the cool dense Ar atmosphere (that is water-cooled) with an estimated cooling rate of 30°C/s. In the dehydration experiments, a piece of natural or experimentally hydrated rhyolitic glass was doubly polished and placed in an open gold capsule. The capsule was clamped into a groove at the tip of a Ni rod. The sample and the rod were then placed in the rapid-quench cold-seal pressure vessel and brought to the specified temperature and pressure. Temperature was measured with a type-K thermocouple with a typical fluctuation of ≤ 3°C over the course of an experiment. The temperature uncertainty, including that associated with the uncertainty in sample position, is estimated to be 10°C.

Dehydration experiments are limited to maximum water of about 4% and mostly to low temperatures. In the dehydration experiments, the steep profile near the surface (often from zero to 1/3 of the maximum H_2O_t concentration, see Fig. 4) cannot be determined. Other experimental problems with dehydration experiments include surface cracking (more severe with increasing H_2O_t, probably owing to volume shrinkage due to water loss), which may enhance H_2O loss, crystallization (at intermediate temperatures below liquidus and above T_g), and flow (at high T and high H_2O_t), which may change the shape of the experimental charge. Hence, in order to better constrain the dependence of $D_{H_2O_t}$ on T and H_2O_t, diffusion-couple experiments were also conducted.

2.1.2. Diffusion-couple experiments

Diffusion-couple experiments were carried out in a vertical internally–heated pressure vessel (IHPV) and a rapid-quench CSV at Universität Hannover, except for Rhy-DC5a that was conducted in a piston cylinder apparatus (PCA) at the University of Michigan. The experimental procedure in IHPV, in general, follows that of Nowak and Behrens (1997).

In each diffusion-couple experiment, two rhyolitic glass cylinders of the same diameter, one containing high H_2O_t (experimentally hydrated) and one containing low H_2O_t (natural sample), were prepared. One of the base surfaces of each cylinder was polished. The two cylinders were placed together so that the polished surfaces are in contact. The interface of some diffusion-couple experiments was marked by a dent or some Pt powder. The diffusion couple was then placed in a gold capsule (or a platinum capsule at $\sim$1200°C, or a graphite capsule for PCA experiment). The gold capsule was manually squeezed to minimize air and free space in the capsule, welded shut, and compressed in Ar gas at room temperature in a CSV. The compressed gold capsule (or the graphite capsule) was then placed in the vessel (or PCA), pressurized, and heated to the experimental temperature for a specific duration. The high-H_2O_t half was on top of the low-H_2O_t half, except for experiments conducted in a horizontal cold-seal pressure vessel (Rhy-DC3 and Rhy-DC4, Table 1).

Table 1
Conditions of diffusion experiments
Duration: If two values are given, the first value indicates the actual duration at the experimental T and the second indicates the effective duration at the experimental T by accounting for diffusion during heating-up and cooling-down. The effective duration is used for the calculation of D.
Initial H_2O_t of the two halves of diffusion-couple experiments are the nominal H_2O_t determined by Karl–Fischer titration on fragments from the same batch of glass prepared in the IHPV.
Thickness is for the final polished slice for IR measurements.
Final H_2O_t: the highest and lowest H_2O_t measured along the diffusion-couple profile. Not given for the dehydration experiments because there is no H_2O loss near the center of the charge.
Comments: IHPV = internally heated pressure vessel; CSV = cold-seal vessel; PCA = piston cylinder apparatus.
Pressure uncertainty is 5 MPa on high-P experiments (except for Rhy-DC5a which has a pressure uncertainty of $\sim$50 MPa) and is negligible for 0.1-MPa experiments. Duration uncertainty is $\sim$30 s. Thickness uncertainty is 2 μm.

Experiment	T (°C)	P (MPa)	Duration (s)	Initial H_2O_t (wt.%)	Thickness (μm)	Final H_2O_t	Comments
Diffusion-couple experiments							
Rhy-DC1	900 ± 10	500	0/120	7.6/0.09	294	7.7/0.08	IHPV[a]
Rhy-DC2	900 ± 10	500	1800/1920	7.6/0.09	291	6.7/0.08	IHPV[b]
Rhy-DC3	696 ± 5	500	720	7.6/0.18	402	7.1/0.20	CSV[c]
Rhy-DC4	853 ± 5	500	240	7.6/0.18	399	7.3/0.20	CSV[c]
Rhy-DC5a	555 ± 10	500	9065/9090	7.6/0.09	229	6.8/0.10	PCA[b,d]
Rhy-DC9	1205 ± 10	500	900/1060	6.4/0.18	238	6.3/0.17	IHPV
Rhy-DC10	862 ± 10	250	1800/1920	6.0/0.09	250	5.8/0.10	IHPV[c,d]
Rhy-DC11	1215 ± 10	250	1200/1360	6.0/0.09	298	6.0/0.10	IHPV
Dehydration experiments							
KS-D12P	602 ± 5	500	263,650	0.79	546		CSV
KS-D13P	595 ± 5	50	167,700	0.81	384		CSV[e]
KS-D14	603 ± 5	0.1	93,160	0.77	479		
KS-D18P	592 ± 5	810	252,900	0.82	389		CSV
KS-D19P	601 ± 5	200	227,760	0.79	398		CSV
KS-D23P	563 ± 5	500	236,800	0.73	373		CSV
KS-D24P	480 ± 10	500	1,067,900	0.87	407		CSV
Rhy-D12P	605 ± 5	500	144,300	1.86	545		CSV
KS & 3-D16P	530 ± 5	500	68,520	3.71	289		CSV
SRhy-DAr1	907 ± 5	500	36,000	0.225	409		CSV
SRhy-DAr2	1025 ± 5	500	14,400	0.219	407		CSV

[a] Temperature was variable during the experiment.
[b] The high-H_2O_t end has lost significant amount of H_2O_t.
[c] The high-H_2O_t end has lost minor amount of H_2O_t.
[d] There are cracks in the experimental charge.
[e] Bubbles grew during the 0.1-MPa experiment.

Ar was used as the pressure medium outside the capsule in IHPV and CSV experiments. The pressure of the IHPV was automatically controlled to within 5 MPa during the experiment and during quench. The pressure uncertainty in the PCA experiment is not exactly known, and is roughly estimated to be 50 MPa.

Fig. 1 shows typical heating and cooling history in IHPV and PCA. Temperature fluctuation was typically below ±5°C in the IHPV experiments. (The Rhy-DC2 curve shown in Fig. 1A has much larger fluctuations and is the worst case because a new furnace was used, and the temperature control was not optimized yet.) In the piston cylinder experiment, the temperature fluctuation was ±2°C (Fig. 1B). The accuracy of the average temperature of the IHPV and PCA experiments, including temperature fluctuation, and the uncertainty in temperature, associated with sample position uncertainty, is estimated to be 10°C. For diffusion-couple experiments in the CSV, the furnace was first heated to the desired temperature and the sample was then moved to the

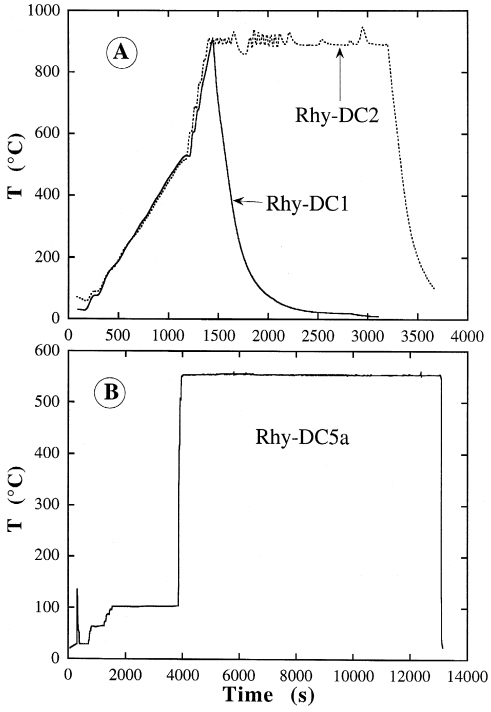

Fig. 1. (A) Thermal history of two diffusion-couple experiments carried using the internally heated pressure vessel. Rhy-DC1 is the nominal zero-time experiment and the duration of Rhy-DC2 at 900 ± 20°C is 1800 s. (B) Thermal history of a diffusion-couple experiment carried out using the PCA (heating at ~ 5 K/s and quenching at ~ 70 K/s). The dwelling temperature is 555 ± 2°C.

hot spot by turning the vessel from a horizontal position to a vertical position. Temperature uncertainty, including that associated with the uncertainty in sample position, is ~ 10°C. The experimental charge was quenched by turning off the power to the IHPV (1–2 K/s; Zhang et al., unpublished data) and PCA (about 70 K/s; unpublished data), and by turning the vessel upside down for CSV experiments (estimated to be about 30 K/s).

Combining the diffusion-couple and the dehydration experiments, a wide range of temperature, pressure, and H_2O_t is covered: 530–1215°C, 0.1–810 MPa, 0.1–7.7% (Table 1).

2.2. Infrared (IR) analyses

After quenching, the wafer was sectioned perpendicular to its polished surface near its center. This provided a glass slice with the complete diffusion profile. The slice was then polished on both surfaces to a typical thickness of 0.2–0.5 mm. H_2O_t, H_2O_m, and OH concentration profiles were determined from IR spectra measured with an IR microscope A590 connected to a FTIR spectrometer Bruker IFS88 at Universität Hannover. A slit aperture between the objective and the detector was used to limit the analysis sample volume. In the focus plane, the area selected by the slit was typically 20 μm wide and 100 μm long, resulting in a spatial resolution of about 30 μm (depending on sample thickness) as determined using a plate with a step-like transition in H_2O content. The sample was fixed to a translation stage. The slice was aligned so that its rim (for dehydration samples) or center line (for diffusion-couple samples) was parallel to the slit. The slice can be moved in both vertical and horizontal directions by micrometer drives. The rim or center position of the wafer was determined with an optical microscope. Once that position has been determined, the distance away from it was determined using the microscope reading when the rim/center is still in the field of view (≤ 180 μm). The precision of this is about 5 μm. Longer distances were determined from the difference between the micrometer reading at the rim/center and the reading at the position measured. Positions measured in this way are reproducible to better than 20 μm in a 1000-μm distance. The calibration of the microscope reading during each measurement is by regressing the microscope reading and the micrometer reading at distances of ≤ 180 μm. Hence, self-consistency of the two methods is insured. There are two difficulties near the edge of a dehydration sample. One is that the edges of the polished slices are never perfectly flat due to chipping during cutting and polishing, and/or due to surficial cracks (likely developed upon quenching and worsened during polishing). Furthermore, the edge may not be perfectly vertical, leading to uncertainties in distance determinations. Hence, the uncertainty in determining the position of the edge for some samples can be larger than 5 μm error discussed above, and H_2O_t concentrations could usually only be measured precisely at more than ~ 30 μm away from the edge, the exact distance depending on the particular glass wafer.

H_2O_m and OH concentrations were determined from the peak height of the absorption bands at 5230

and 4520 cm^{-1}. For dehydration experiments, the maximum H_2O_t is $\leq 4\%$ and the calibration of Zhang et al. (1997) is used for the calculation of H_2O_m, OH, and H_2O_t concentrations. The baseline is fit by a flexicurve. The calibration of Zhang et al. (1997) used only sample with less than 5.5% H_2O_t and the best calibration is for $H_2O_t \leq 2.7\%$ as assessed by the authors themselves. Hence, extrapolation to higher H_2O_t may not be very accurate owing to the complexity of the calibration. Furthermore, the differences between Karl–Fischer titration results and the calibration of Zhang et al. (1997) increases rapidly at high H_2O_t: 3.81% vs. 3.64%; 5.64% vs. 5.25%; and 7.66% vs. 6.59% (unpublished data). For diffusion-couple samples, the concentration at high H_2O_t is as high as 7.7%. Hence, we used the calibration of Withers and Behrens (1999) for the diffusion-couple samples. In this calibration, a straight line is fit to the baseline of the 5230 cm^{-1} peak and extrapolated to that of the 4520 cm^{-1} peak (see Behrens et al., 1996). The relative precision of the analyses for H_2O_t is about 5%. Because diffusivities are largely dependent on the relative concentration differences, not so much on the absolute concentration, the uncertainty in the calibration is not expected to affect the extracted diffusivity in a major way. However, the different calibration is expected to affect speciation studies significantly.

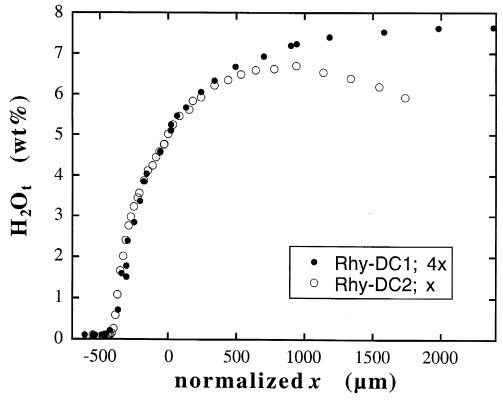

Fig. 2. Comparison of the two diffusion profiles at 900 ± 10°C and 500 ± 5 MPa. The normalized distance for Rhy-DC1 is the original distance multiplied by four and that for Rhy-DC2 is the original distance. During the experiment, the high-H_2O_t side of sample Rhy-DC2 lost H_2O from the surface and the low-H_2O_t side gained water (noticeable at $x < -1600$ μm). The middle part of the Rhy-DC2 profile is unaffected, and hence, can be compared with Rhy-DC1. There are more points of Rhy-DC1 outside the distance region, which are not shown so that the comparison is not compressed.

3. Experimental results

3.1. Diffusion profiles

Diffusion profiles are measured for eight diffusion couple experiments, and 11 dehydration experiments. Two out of the 11 dehydration experiments are from Ar sorption experiments (to be reported elsewhere). Because the initial samples contain some H_2O, there is also a dehydration profile beside the Ar profile. Several other experiments are classified as unsuccessful and not reported because of significant bubble or crystal growth, or severe cracking, or rupture of the capsule. Table 1 lists the experimental conditions. Most experimental H_2O diffusion profiles obtained in this study are shown in Figs. 2–4. The figures are explained in more detail below. Only H_2O_t profile is shown because the temperature in many experiments is high so that H_2O_m and OH profiles are not expected to reflect those at the experimental temperature. The local species concentrations are expected to record those at an apparent equilibrium temperature lower than the experimental temperature for many experiments.

3.2. Effective duration at the experimental temperature

The durations of diffusion-couple experiments at the intended temperature range from 240 to 9100 s, whereas the heating up and cooling down typically take ~ 2000 s. In order to examine the effect of diffusion during heating up and cooling down, a ''zero''-time experiment was carried out in IHPV at 900°C and 500 MPa with initial high H_2O_t of 7.7% and initial low H_2O_t of 0.08%, to be compared with a similar experiment but with a nominal duration of 1800 s. The thermal histories of the two experiments are shown in Fig. 1A. The effective duration of the experiments was obtained in two ways.

(1) In the first method, the diffusivity as a function of T (and hence, t) is integrated with respect to

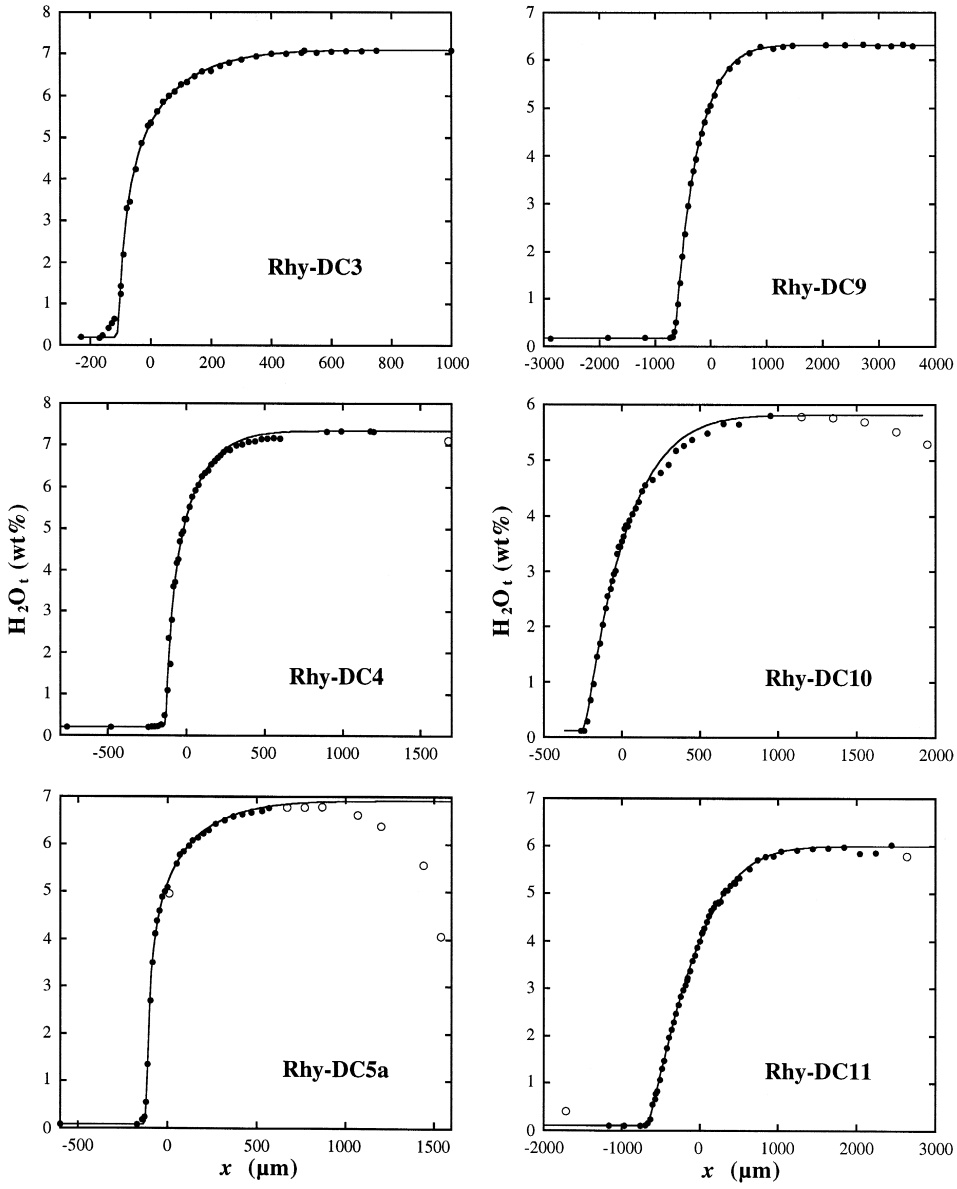

Fig. 3. Diffusion-couple profiles (here and Fig. 2). Also shown are fits (to be discussed later in the text) using $D_{H_2O_m} = D_0 \exp(aX)$ and $a = -27.21 + 36{,}892/T + 57.23P/T$ where P is in megaPascal and T is in Kelvin. The best-fit D_0 values are listed in Table 3. Only the solid points are used in the fits. The data shown in open circles are affected either by H_2O loss or gain, or close to a crack.

time. The result is divided by D at the intended experimental temperature (900°C). The result, $\int D\mathrm{d}t/D_{T_{exp}}$, is the effective time at the experimental T. The uncertainty in this treatment is from that in the activation energy of diffusion, which likely varies with H_2O_t when H_2O_t range is large (Nowak and Behrens, 1997; later discussion). Assuming an average activation energy of 80 kJ/mol for H_2O_t diffusion, the effective duration of the ''zero''-time experiment is 121 s for Rhy-DC1. Letting the activation energy vary between 60 and 100 kJ/mol, the corresponding duration varies from 157 to 101 s.

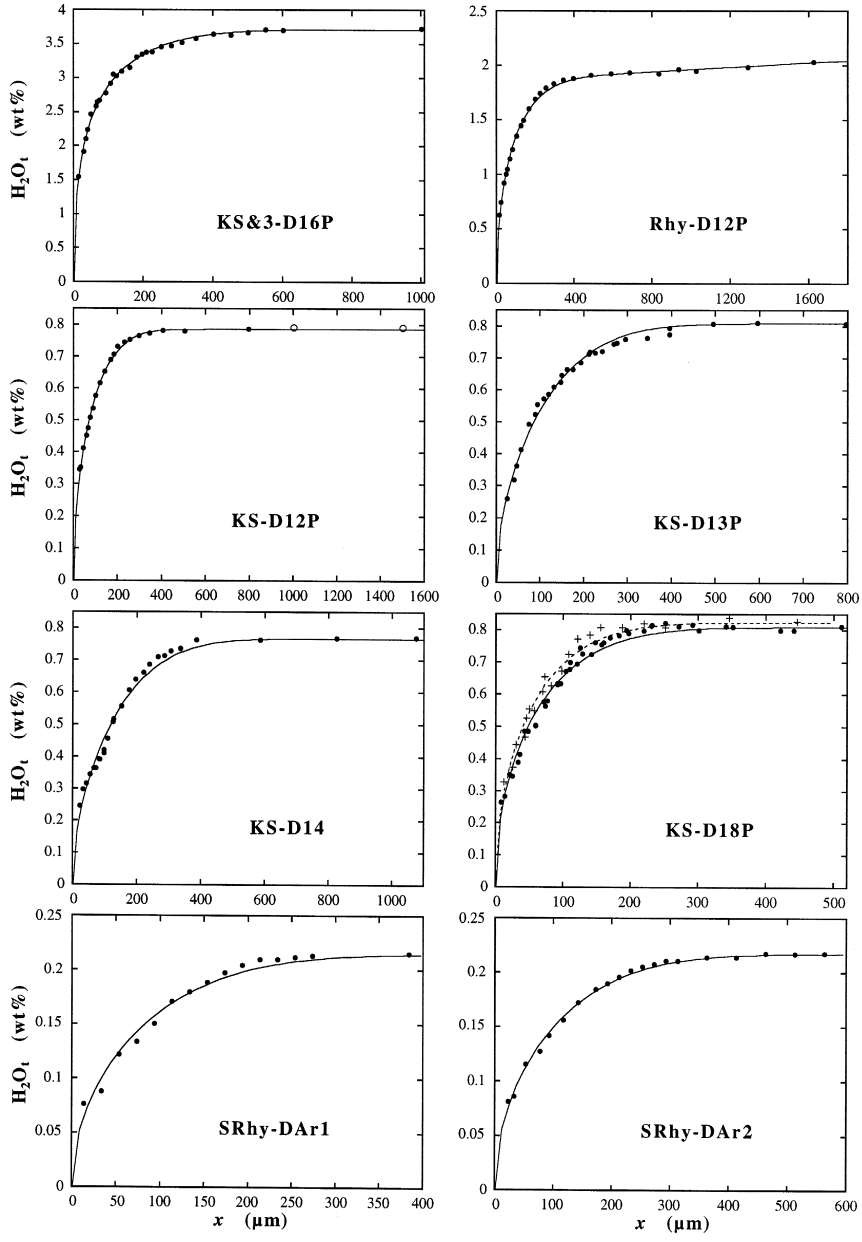

Fig. 4. Dehydration profiles (eight out of 11 are shown) covering variable H_2O_t, pressure, and temperature. Fits are also shown. For Rhy-D12P, the data are fit by a linear trend (to account for initial heterogeneity) plus the calculated diffusion profile to the data. For KS-D12P, the two data points shown as open circles are not used in fitting because these may represent initial heterogeneity. For KS-D18P, two profiles are measured and both fits are shown.

(2) The second method of obtaining the effective duration of the ''zero''-time experiment is by comparing its experimental profile with the profile of Rhy-DC2 (the same T, P, and H_2O_t range but with 1800 s duration). Fig. 2 shows that when the actual diffusion distance of Rhy-DC1 is multiplied by four, the diffusion profile is comparable to the profile of Rhy-DC2 (the decrease of H_2O_t at the far right-hand

side of Rhy-DC2 is owing to H_2O loss discussed in the figure caption and later). Therefore, the effective duration for Rhy-DC2 is 16 times that of Rhy-DC1. The effective duration for Rhy-DC1 can hence be solved from $(t + 1800)/t = 16$, resulting in a duration of 120 s. The effective duration for Rhy-DC2 is thus $1800 + 120 = 1920$ s.

Combining the two approaches, the effective duration for Rhy-DC1 and Rhy-DC2 is 120 ± 30 s plus the time dwelling at the experimental temperature. For other experiments, the effective duration is obtained by adding a duration calculated from heating and cooling history using an activation energy of 80 kJ/mol. Two diffusion-couple experiments were carried out using a cold-seal pressure vessel and the experimental charge was moved to the hot spot after the experimental temperature was reached and quenched by moving the charge to the cold end of the pressure vessel. Although the exact thermal history could not be recorded, the heating-up and cooling-down times roughly cancel each other and the net effect on the effective duration is ignored. Table 1 shows both the nominal and the effective durations of diffusion-couple experiments when there is a significant difference.

For dehydration experiments, the heating-up time is about 30 min and the quenching time is negligible. By estimating $\int D\mathrm{d}t/D_{T_{exp}}$, the effective duration owing to heating-up is about 375 s, $\leq 0.5\%$ of the duration at the experimental temperature. Hence, no correction is made to the experimental duration.

3.3. Some problems

Dehydration experiments only provide constraints to H_2O diffusion at relatively low H_2O_t, which can be roughly modeled by a constant $D_{H_2O_m}$. In order to examine the H_2O diffusion behavior in a large H_2O_t range, the diffusion-couple experiments provide best constraints owing to the large H_2O_t range that a profile covers. Hence, much of the constraint on H_2O diffusion is obtained from these profiles. Unfortunately, the diffusion-couple experiments are more complicated and more prone to experimental problems. The comparison of two diffusion profiles (Rhy-DC1 and Rhy-DC2) in Fig. 2 shows some of the problems. The concentration profile of the ''zero''-time experiment Rhy-DC1 is not affected by H_2O loss from the high-H_2O_t side, nor H_2O gain by the low-H_2O_t side during the experiment. However, for Rhy-DC2, the highest H_2O_t at the high-H_2O_t side is significantly lower than the initial high H_2O_t, and H_2O_t decreases with increasing x when x is greater than 1000 μm (Fig. 2), indicating H_2O loss from the high-H_2O_t surface (right-hand side at $x \approx$ 1800 μm in Fig. 2). It is also possible that some H_2O is lost from the cylindrical side of the charge during the experiment. Although not shown in Fig. 2, the low-H_2O_t side of Rhy-DC2 gained H_2O. Nevertheless, owing to slow diffusion rate in the low-H_2O_t side, there is a large and well-resolved region of constant low-H_2O_t similar to the initial low-H_2O_t. Hence, the gain does not affect the diffusion profile. However, the loss of H_2O_t from the high-H_2O_t side presents a main problem to our experiments.

To minimize H_2O_t loss, the experimental duration was minimized. However, the experimental duration at the experimental T must be significantly longer than 120 s, so that the diffusion profile can be treated to be diffusion at constant T and that the dependence of the D–H_2O_t relation at a constant T can be examined (see later discussion). Hence, H_2O loss is still a problem although it is not so severe as in the experiments of Nowak and Behrens (1997). Furthermore, the necessary short duration also leads to significant uncertainty in the effective experimental duration (see above), and to steep profiles at the low-H_2O_t side which are difficult to resolve. The poor fit of the profile of Rhy-DC3 at low H_2O_t (Fig. 3) is likely owing to the convolution effect (Ganguly et al., 1988).

The loss of H_2O_t at the high-H_2O_t side and the gain at the low-H_2O_t side in IHPV and CSV are not owing to capsule rupture (experiments with ruptured capsule were classified as unsuccessful and not reported). The likely cause is vapor phase transportation in the capsule. Although the capsule was squeezed and compressed before the experiment, there is likely still some air and free space between the capsule and the experimental cylinders. Hence, during the experiment, there was a free vapor phase that could transfer H_2O from the high-H_2O_t side to the low H_2O_t-side.

Other problems with the diffusion-couple experiments include cracks in the experimental charges

(Rhy-DC5a, and another piston cylinder charge that is much more severely cracked and hence, not reported), leading to uncertainties in estimating the diffusion distance. There is also the uncertainty with possible but unknown complications in more complicated experiments.

3.4. Electron microprobe results

One diffusion couple (Rhy-DC2) was analyzed for major oxide concentrations by a Cameca electron microprobe at the University of Michigan. The analyses were carried out at 15 kV with a 3-nA defocused beam of 6 μm diameter, following the procedure of Zhang et al. (1997). To counter Na loss problem during microprobe analysis, Na was analyzed for five periods, each for 6 s, and Na concentration was obtained by extrapolating the counting rate to zero time. This procedure avoids systematically low Na concentration but reduces the precision of Na data. Fig. 5 compares H_2O_t determined by IR and difference (100 − total) of the microprobe analyses (i.e., the difference between 100% and the total is attributed to H_2O_t). For this comparison, the positions of the points must be consistent between IR and microprobe analyses. The consistency is obtained by sliding the two profiles so that they roughly match, as shown in Fig. 5. The error in determining the interface position by this method is in the order of 50 μm, owing to large relative uncertainties in microprobe (100 − total) values. Fig. 5 shows that

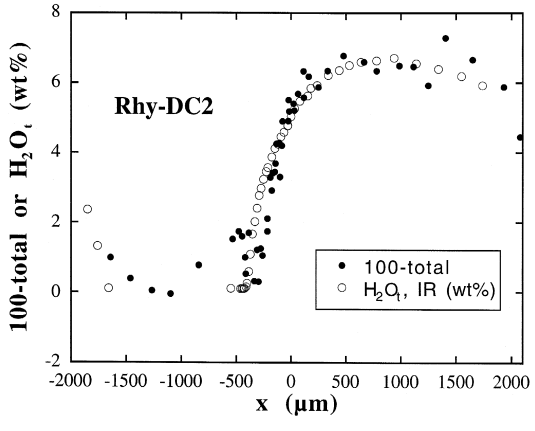

Fig. 5. H_2O_t determined by IR compared to 100 − total of microprobe analyses.

H_2O_t determined from the microprobe difference (100 − total) is roughly in agreement with the IR determination. The individual oxide concentration profiles have relatively large errors and are not shown. In Section 4 below, H_2O diffusion is treated as effective binary diffusion (Lapham et al., 1984; Watson, 1994; Nowak and Behrens, 1997; Mungall et al., 1998).

4. Discussion

4.1. Modeling H_2O diffusion

One important issue we address is how H_2O diffusivity varies with H_2O_t at a given T and P. At low H_2O_t ($< 2\%$ H_2O_t), the diffusion can be either modeled by H_2O_t-independent $D_{H_2O_m}$ and negligible D_{OH} (Zhang et al., 1991a), or phenomenologically described by a $D_{H_2O_t}$ proportional to H_2O_t content (Zhang et al., 1991a; Nowak and Behrens, 1997; Zhang and Behrens, 1998). The two descriptions are roughly equivalent at low H_2O_t because dX_m/dX is roughly proportional to H_2O_t (Zhang et al., 1991a). When H_2O_t content is greater than 2%, our new data at 500 MPa show that this simple model of Zhang et al. (1991a) does not apply anymore, which is in agreement with Nowak and Behrens (1997). The relation between $D_{H_2O_t}$ and H_2O_t to 8% H_2O_t is the main focus of this section.

At high H_2O_t, the dependence of $D_{H_2O_t}$ on H_2O_t is best examined using the diffusion-couple profiles because the large H_2O_t range across a diffusion profile is necessary for constraining how $D_{H_2O_t}$ depends on H_2O_t. In order to constrain how $D_{H_2O_t}$ (or $D_{H_2O_m}$) varies with H_2O_t to 7.7% H_2O_t, either the Boltzmann–Matano method can be used, or a functional relation between the diffusivity and H_2O_t can be specified and then verified by fitting the experimental diffusion profile. Both approaches have their pros and cons. The Boltzmann–Matano method is independent of assumptions of the diffusion mechanisms. However, this method does not give reliable diffusivity at the low and high H_2O_t ends of the profile (Zhang and Stolper, 1991; Nowak and Behrens 1997). Using a functional relation between diffusivity and H_2O_t to fit the profiles potentially has

much higher precision (Zhang et al., 1991a). However, this approach is dependent on assumptions on the diffusion mechanisms and on the speciation in the melt. We emphasize the latter approach to analyze H_2O diffusion in silicate melts because it potentially has much higher precision.

In order to specify a functional relation between the diffusivity and H_2O_t, we must consider the possible causes for the variation of $D_{H_2O_t}$ with H_2O_t. In the context of two-species diffusion, the rapid increase of $D_{H_2O_t}$ with H_2O_t at high H_2O_t can be attributed to either an increase of $D_{H_2O_m}$ with H_2O_t, or a significant contribution of OH to the diffusion and hence, a much more rapid increase of D_{OH} with H_2O_t, or both. Furthermore, other mechanisms can also be constructed. For example, Behrens and Nowak (1997) proposed that the formation of OH pairs may contribute significantly to H_2O_t diffusion. Mathematically, the role of OH pairs is equivalent to that of H_2O_m in affecting the shape of diffusion profiles because both the concentrations of OH pairs and that of H_2O_m are proportional to the square of OH concentration. Hence, whether OH pairs contribute to H_2O diffusion will not be examined further because its role cannot be resolved from diffusion profiles. Because none of the species diffusivities is constant, mathematically, either the variation of $D_{H_2O_m}$ with H_2O_t, or the variation of D_{OH} with H_2O_t (or both) would be able to describe the required $D_{H_2O_t}$ variation with H_2O_t at high H_2O_t. However, for OH contribution to dominate the diffusion at high H_2O_t is unlikely because OH/H_2O_m ratio decreases with increasing H_2O_t and because it is unlikely that the diffusivity of OH would exceed that of H_2O_m. Therefore, in our effort to model H_2O diffusion profiles, we will mainly consider the model in which the variation of $D_{H_2O_t}$ with H_2O_t is caused by the variation of $D_{H_2O_m}$ with H_2O_t. This is also the simplest model (in that only one species is diffusing) that can accommodate the available diffusion data.

There may be subspecies of H_2O_m and OH (e.g., Kohn et al., 1989; Sykes and Kubicki, 1993), which may affect our mechanistic understanding of H_2O diffusion. However, as long as the subspecies are in equilibrium and hence, proportional to each other, they do not affect the mathematical modeling of H_2O_t diffusion. For example, Zhang et al. (1991b) showed that the role of CO_2 and CO_3^{2-} in contributing to the diffusion cannot be resolved from the measured carbon diffusion profiles as long as their concentrations are proportional.

A reasonable and relatively simple assumption for the dependence of $D_{H_2O_m}$ on H_2O_t is that $D_{H_2O_m}$ is an exponential function of H_2O_t (or ln $D_{H_2O_m}$ is linear to H_2O_t):

$$D_{H_2O_m} = D_0 \exp(aX), \tag{3}$$

where D_0 is $D_{H_2O_m}$ as H_2O_t concentration approaches zero, and X is the mole fraction of H_2O_t (on single oxygen basis), and a is a parameter to be determined. Knowing how X_m depends on X (e.g., Eq. 13 of Zhang, 1999, if local equilibrium is reached), dX_m/dX can be expressed as:

$$\frac{dX_m}{dX} = \frac{16X}{b} - \frac{8X^2}{b^2}\left[8 - 2K + \frac{8K - 2K^2(1-2X) - 16KX}{\sqrt{[K(1-2X)]^2 + 16KX(1-X)}}\right], \tag{4}$$

where K is the equilibrium constant for the species interconversion reaction (Reaction R1) and is calculated from $K = 6.53e^{-3110/T}$ (Zhang et al., 1997), and $b = 8X + K(1-2X) + \sqrt{[K(1-2X)]^2 + 16KX(1-X)}$. Hence, $D_{H_2O_t}$ can be calculated using Eq. (2) with $D_{H_2O_m}$ from Eq. (3) and dX_m/dX from Eq. (4). With this model, at low H_2O_t, $D_{H_2O_m}$ is roughly constant and hence, $D_{H_2O_t}$ is proportional to H_2O_t content, consistent with the results of Zhang et al. (1991a) and Nowak and Behrens (1997), and results of this study for low-H_2O_t profiles (Zhang and Behrens, 1998). At high H_2O_t, $D_{H_2O_m}$ increases exponentially with H_2O_t. Because dX_m/dX does not vary much at high H_2O_t, $D_{H_2O_t}$ also increases exponentially with H_2O_t. This is consistent with the high H_2O_t data of Nowak and Behrens (1997). The verification of this assumption comes from two sources: one is the ability to fit H_2O_t diffusion profiles in this study and reconcile all diffusion data (see below), and the second is our preliminary data of the diffusivity of Ar (a molecular species) in silicate melts showing D_{Ar} (diffusivity of

a molecular species) to be an exponential function of H_2O_t (to be published elsewhere).

To fit the diffusion profiles using the above expression for $D_{H_2O_m}$, we need to know whether local species equilibrium is reached during the experiment. At temperatures ≥ 600°C and $H_2O_t \geq 2\%$, equilibration between H_2O_m and OH is rapid (< 20 s, Zhang et al., 1995) and can be safely assumed. The equilibrium constant at the temperature is extrapolated from the results of Zhang et al. (1997). Hence, there are two adjustable parameters in fitting the diffusion profile, D_0 and a. A third adjustable parameter is Δx_0, the position of the Boltzmann–Matano interface relative to the marked interface. (Sometimes, the interface is not marked; hence, only the Boltzmann–Matano interface position, but not Δx_0, can be found.) For every given a value, and initial H_2O_t contents on both halves, a diffusion-couple profile is calculated by modifying the program of Zhang et al. (1991a) to account for the dependence of $D_{H_2O_m}$ on X. This calculated diffusion profile is used to fit the diffusion data by adjusting D_0 and Δx_0. When a value varies, both D_0 and Δx_0 vary. The a value that leads to the best fit is found by trial-and-error. Fig. 6 shows the fit of a diffusion-couple profile and the effect by changing a. The best-fit a value is obtained to be 17.4. Using a similar approach of trial-and-error, the best-fit a value can be obtained from each diffusion-couple profile and from a dehydration profile with high initial H_2O_t (KS and 3-D16P). Table 2 reports all best-fit a values.

Because our method of obtaining a is through trial-and-error, it does not allow a quantitative estimation of the uncertainty for the a-value. Furthermore, no simple method can account for errors associated with experimental problems of H_2O loss. Therefore, a qualitative evaluation (grades A, B, C, and D, corresponding to worsening accuracy) is assigned to the accuracy of each a value based on whether there are complexities in the diffusion profiles. When both the high low-H_2O_t ends have a large region of flat concentration profile (meaning H_2O_t loss or gain does not affect the concentrations at the ends), the profile constrains a value best, and the quality of the constraint is assigned to be A. Although the H_2O_t content at the high-H_2O_t side of Rhy-DC3 and Rhy-DC4 is lower than the initial 7.6%, indicating loss of H_2O (possibly from the side

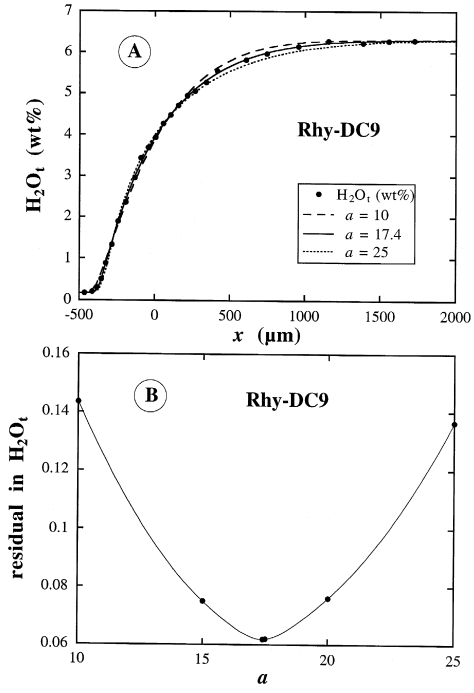

Fig. 6. (A) Fitting a diffusion-couple profile (Rhy-DC9, 1205°C, 500 MPa, 900 s) using different a values. For clarity, data points at the far left and far right sides are not shown; they are shown in Fig. 3. (B) The variation of the average fit residual vs. the a value, to show how the quality of the fit depends on the a value. The best fit is at $a = 17.4$.

of the cylindrical charges), there is a large flat region. Hence, the possible loss is assumed to have only a minor effect on the constraint of the a value. When there is also a minor convolution effect coupled with lower-than-initial high H_2O_t (Rhy-DC3), the quality is B. When H_2O_t loss is visible (Rhy-DC10), then the quality is C. For the zero-time experiment Rhy-DC1, although there is no H_2O_t loss from the ends, it is not a constant-temperature experiment and hence, the quality is also assigned to be C. When H_2O_t loss is significant, the quality is D. One dehydration experiment with highest initial H_2O_t of 3.7% is also used to constrain a. In this case, there is no constraint on the low-H_2O_t portion and hence, the quality of constraint on a is D. In order to obtain the dependence of a on T and P, it is necessary to quantify the error of each letter grade assignment. We arbitrarily assign 5% relative error to grade A, 10% to B, 20% to C, and 40% to D. The qualitative

Table 2
Results of best-fit a values by fitting diffusion profiles assuming $D_{H_2O_m} = D_0 \exp(aX)$
In fitting the diffusion profile, H_2O_m concentration at the experimental temperature is calculated from H_2O_t and species equilibrium constant K at the temperature ($K = 6.53e^{-3110/T}$, Zhang et al., 1997).

Experiment	T (°C)	P (MPa)	Effective duration (s)	best a	r^2	Quality
Rhy-DC9	1205	500	1060	17.4	0.9998	A
Rhy-DC1	900	500	120	31	0.9977	C
Rhy-DC2	900	500	1920	significant H_2O_t loss, $a \sim 31$		D
Rhy-DC4	853	500	240	36.2	0.9963	A
Rhy-DC3	696	500	720	40	0.9976	B
Rhy-DC5a	550	500	9090	significant H_2O_t loss, $a \sim 50$		D
KS and 3-D16P	530	500	68,520	low-H_2O_t part is missing, $a \sim 58.9$		D
Rhy-DC11	1215	250	1360	7.12	0.9993	A
Rhy-DC10	862	250	1920	24.4	0.9984	C

assignment is used below for obtaining a general expression of $D_{H_2O_m}$. From Table 2, the best-fit a values depend on T and P even when these generously assigned uncertainties are taken into account.

4.2. H_2O_m diffusion as a function of T, P and X

In order to determine the relation between $D_{H_2O_m}$, T, P, and X, it is necessary to specify how the parameter a varies with T and P (Table 2). The typical expression for diffusivity as a function of T and P is:

$$D = \exp(a_0 + a_1/T + a_2 P/T),$$

where a_1 is related to the activation energy for diffusion, and a_2 is related to the activation volume. The fact that the parameter a depends on both T and P means that a_0, a_1, and a_2 all depend on X. Therefore, the simplest expression accounting for the observation for each of the parameters above depends linearly on X:

$$D_{H_2O_m} = \exp\left[(a_0 + b_0 X) + (a_1 + b_1 X)/T + (a_2 + b_2 X) P/T\right], \quad (5)$$

or:

$$D_{H_2O_m} = \exp\left[(a_0 + a_1/T + a_2 P/T) + (b_0 + b_1/T + b_2 P/T) X\right]. \quad (6)$$

Comparing Eqs. (3) and (6), we obtain:

$$D_0 = \exp(a_0 + a_1/T + a_2 P/T) \quad (7)$$

and

$$a = b_0 + b_1/T + b_2 P/T. \quad (8)$$

Using the a values in Table 2 (low-pressure data of Zhang et al., 1991a do not provide much constraint for a values because of the low H_2O_t) and accounting for the error associated with each a value as explained above, we obtain:

$$a = -27.21 + 36{,}892/T + 57.23P/T, \quad (9)$$

where T is in Kelvin and P is in megaPascal. The above equation is most accurate at $P = 500$ MPa because most experimental diffusion-couple data are obtained at this pressure. The relation between a and P is not well-constrained owing to limited data. It can be noted from the above equation that a increases with pressure and decreases with temperature, implying that $D_{H_2O_m}$ depends more on H_2O_t at high pressure (and/or low temperatures) than at low pressures (and/or high temperatures). At 0.1 MPa, the dependence of $D_{H_2O_m}$ on H_2O_t is not very pronounced, even at the low temperatures that Zhang et al. (1991a) carried out the experiments, in agreement with the weak dependence of $D_{H_2O_m}$ on H_2O_t over the small concentration range investigated by Zhang et al. (1991a).

Using the above expression for a, all diffusion profiles are refit using the calculated a value instead of the best-fit a value. In order to improve the resolution of the pressure effect, the experimental results of Zhang et al. (1991a) at 0.1 MPa, 403–530°C and 0.1–1.7% H_2O_t are also refit to constrain $D_{H_2O_m}$. The H_2O_t concentrations of these experiments are recalculated using the calibration of Zhang et al. (1997), bringing the species equilibrium constant consistent with that used in this work. For most experiments, the temperature is high and species equilibrium can be assumed. However, some of the dehydration experiments are conducted at relatively low temperatures (< 550°C) and species equilibrium may not have been achieved at low H_2O_t. For these experiments and for experiments of Zhang et al. (1991a), the quotient $Q = X_{OH}^2/[X_m X_O]$ is found to be well-represented by an exponential function $Q = K + \alpha \exp(-\beta X)$ with α and β obtained from actual measured species concentrations (Q represents

Table 3
Results of best-fit ln D_0 values by fitting diffusion-profile fits assuming $D_{H_2O_m} = D_0 \exp(aX)$.
The fits shown in this table are different from those in Table 2 because the parameter a in $D_{H_2O_m} = D_0 \exp(aX)$ is obtained using $a = -27.21 + 36{,}892/T + 57.23P/T$ where P is in megaPascal and T is in Kelvin. (In Table 2, a is varied to find the best fit.)
Error in ln D_0 is given at the 2-s level and includes only those from the fits and from the uncertainty in time.
Δx_0 for diffusion-couple experiments reflects (i) error in measuring the actual interface position (including non-vertical interface), and (ii) the difference between the Boltzmann–Matano interface and the actually marked interface. For dehydration experiments, Δx_0 is also allowed to vary because there may be some measurement error in the edge position owing to micrometer precision (5 μm) and imperfect edge (cracks, and non-vertical edge surface).
Two profiles were measured for KS-D18P and both results are used.
Source of data: (1) = this work; (2) = Zhang et al. (1991a).

Experiment	T (°C)	P (MPa)	maximum H_2O_t (wt.%)	ln D_0, D in $\mu m^2/s$	Δx_0 (μm)	r^2 (s)	Source
Diffusion-couple experiments							
Rhy-DC9	1205	500	6.3	3.95 ± 0.04	–	0.9998	1
Rhy-DC1	900	500	7.7	1.99 ± 0.28	4.8	0.9975	1
Rhy-DC4	853	500	7.3	1.68 ± 0.17	19	0.9960	1
Rhy-DC3	696	500	7.1	−0.70 ± 0.11	25	0.9975	1
Rhy-DC5a	555	500	6.8	−3.71 ± 0.08	18	0.9985	1
Rhy-DC11	1215	250	6.0	4.92 ± 0.03	–	0.9993	1
Rhy-DC10	862	250	5.8	2.23 ± 0.07	−9.4	0.9963	1
Dehydration experiments							
KS-D18P.1	592	810	0.82	−3.37 ± 0.11	−7.6	0.9834	1
KS-D18P.2	592	810	0.82	−3.65 ± 0.23	−4.1	0.9748	1
SRhy-DAr2	1025	500	0.22	3.02 ± 0.10	13	0.9956	1
SRhy-DAr1	907	500	0.22	1.42 ± 0.19	−3.5	0.9830	1
Rhy-D12P	605	500	1.86	−2.85 ± 0.07	4.3	0.9978	1
KS-D12P	602	500	0.79	−2.62 ± 0.07	−4.3	0.9978	1
KS-D23P	563	500	0.73	−3.33 ± 0.14	11	0.9883	1
KS and 3-D16P	530	500	3.71	−4.04 ± 0.07	1.2	0.9954	1
KS-D24P	480	500	0.86	−5.10 ± 0.10	15	0.9943	1
KS-D19P	601	200	0.79	−5.10 ± 0.12	2.9	0.9869	1
KS-D13P	595	50	0.81	−1.58 ± 0.11	−5.1	0.9902	1
KS-D14	603	0.1	0.77	−0.50 ± 0.16	4.9	0.9838	1
KS-D2	530	0.1	0.84	−2.47 ± 0.17	−28	0.9909	2
PD-D5	530	0.1	0.22	−2.09 ± 0.14	6.6	0.9890	2
KS-D3	490	0.1	0.82	−3.21 ± 0.07	5.8	0.9978	2
PD-D4	490	0.1	0.19	−3.14 ± 0.18	−7.2	0.9928	2
KS-D5A	450	0.1	0.82	−4.10 ± 0.09	12.2	0.9958	2
3b-D4N	403	0.1	1.68	−5.08 ± 0.07	7.3	0.9984	2
3b-D4	403	0.1	1.29	−5.36 ± 0.08	−16	0.9968	2
KS-D4A	403	0.1	0.82	−5.83 ± 0.23	−20	0.9850	2

the quotient regardless of equilibration, and K is Q at equilibrium). Hence, the exponential expression of Q is used in fitting these low-temperature profiles. This approach using the actual measured Q is similar to that used in Zhang et al. (1991a).

Most fits are shown in Figs. 3 and 4. The best D_0 values (recall that D_0 is $D_{H_2O_m}$ as H_2O_t approaches zero) are listed in Table 3 and plotted in Fig. 7. It is important to note that D_0 should be independent of the total H_2O_t covered by an experiment. Indeed, Fig. 7 shows that ln D_0 vs. $1/T$ at a given P forms a consistent trend, independent of dehydration and diffusion-couple experiments, and independent of the maximum H_2O_t in the experiment, demonstrating inter-experimental reproducibility. For example, D_0 values for Rhy-DC9 (diffusion-couple experiment with H_2O_t range of 0.1–7%) and SRhy-DAr2 (dehydration experiment with maximum H_2O_t of only 0.2%) lie consistently in the same trend. Hence, we conclude that the expression of $D_{H_2O_m} = D_0 \exp(aX)$ captures the essence of the variation of $D_{H_2O_m}$ with H_2O_t.

The D_0 values (in $\mu m^2/s$) in Table 3 are fit to obtain:

$$\ln D_0 = 14.08 - 13{,}128/T - 2.796P/T. \quad (10)$$

The above equation reproduces all ln D_0 values to within 0.5 (i.e., it reproduces D_0 values to within a factor of 1.7). The value of D_0 decreases with increasing pressure (Fig. 7). For example, using the above equation, at 600°C, D_0 is 0.40 $\mu m^2/s$ at 0.1 MPa and 0.076 $\mu m^2/s$ at 500 MPa, varying by a factor of 5.

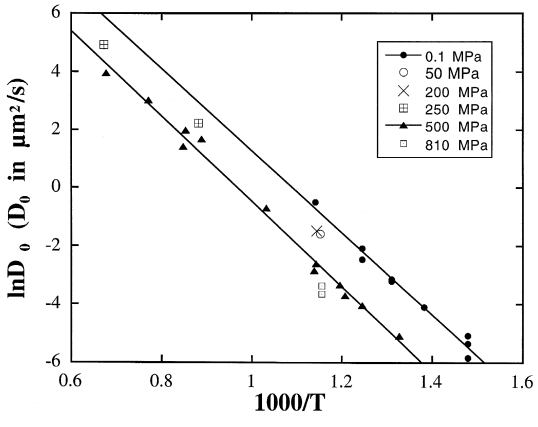

Fig. 7. All D_0 data shown as a function of temperature (in an Ahrrenius plot) and pressure. The r^2 value is 0.981 for fitting the 0.1-MPa data and 0.992 for fitting the 500-MPa data.

Combining Eqs. (9) and (10), we have:

$$D_{H_2O_m} = \exp\left[(14.08 - 13{,}128/T - 2.796P/T) + (-27.21 + 36{,}892/T + 57.23P/T)X\right], \quad (11)$$

where T is in Kelvin, P is in megaPascal, and $D_{H_2O_m}$ is in micrometer squared per second. From the above equation, the activation energy for H_2O_m decreases with increasing H_2O_t and depends on pressure. At low H_2O_t and 0.1 MPa, it is 109 kJ/mol, similar to 103 kJ/mol obtained by Zhang et al. (1991a). At 500 MPa and 6.0% H_2O_t, the activation energy for H_2O_m diffusion is 65 kJ/mol, implying an activation energy of 59 kJ/mol for H_2O_t diffusion, similar to the results by Nowak and Behrens (1997). The activation volume for H_2O_m also decreases with increasing H_2O_t.

Knowing $D_{H_2O_m}$, $D_{H_2O_t}$ can be calculated using Eqs. (2) and (4). Owing to the pressure and X term in Eq. (11), the H_2O_t diffusivity at a given H_2O_t and temperature can decrease or increase with increasing pressure. For example, at 1% H_2O_t and 600°C, $D_{H_2O_t}$ is 0.19 $\mu m^2/s$ at 0.1 MPa and 0.070 $\mu m^2/s$ at 500 MPa, decreasing by 63%; at 3% H_2O_t and 800 °C, $D_{H_2O_t}$ is 4.6 $\mu m^2/s$ at 100 MPa and 5.1 $\mu m^2/s$ at 600 MPa, only a negligible increase; at 5% H_2O_t and 800°C, $D_{H_2O_t}$ is 10.5 $\mu m^2/s$ at 200 MPa and 28.8 $\mu m^2/s$ at 700 MPa, increasing by 174%.

4.3. Expression for $D_{H_{2t}^O}$

Although it is simple to use Eq. (11) to calculate $D_{H_2O_m}$, it should be noted that the diffusion profiles only constrain $D_{H_2O_t}$. The values of $D_{H_2O_m}$ are dependent on (i) whether other species (such as OH groups or OH pairs) contribute to the diffusion of the H_2O component, and (ii) the speciation model used. In the above modeling, the speciation model of Zhang et al. (1997) is extrapolated far from the

temperature and H_2O_t range of the speciation experiments, which may lead to some errors in the true diffusivities of molecular H_2O species.

Eqs. (2), (4), and (11) can be used to calculate $D_{H_2O_t}$ in a wide range of T, P, and H_2O_t conditions, and the $D_{H_2O_t}$ values calculated this way are model-independent and are consistent with the experimental data as long as self-consistency is maintained. For convenience, $\log_{10} D_{H_2O_t}$ values at selected T, P, and H_2O_t are listed in Table 4. Fig. 8 shows how $D_{H_2O_t}/X$ values change as a function of H_2O_t at several T and P values. If $D_{H_2O_t}$ is proportional to H_2O_t, $D_{H_2O_t}/X$ at a given T and P would be constant. Fig. 8 shows that at 0.1 MPa, $D_{H_2O_t}/X$ does not depend strongly on H_2O_t, which results from the weak dependence of $D_{H_2O_m}$ on H_2O_t (i.e., a small a value). At 500 MPa, $D_{H_2O_t}/X$ increases strongly with H_2O_t, especially at low temperatures (such as 400°C). Nevertheless, the calculation of $D_{H_2O_t}$, which is necessary in modeling H_2O diffusion, is complicated. Furthermore, this formulation requires knowledge on H_2O speciation, and hence, is difficult to extend to other melt compositions (such as dacite, andesite, albite melts).

In order to simplify the calculation for $D_{H_2O_t}$, we develop two direct expressions for the dependence of $D_{H_2O_t}$ on T, P, and X. The first simple expression is applicable for $H_2O_t \leq 2\%$, and the second more complicated expression is applicable to $H_2O_t \leq 8\%$. At $H_2O_t \leq 2\%$, the approximation that $D_{H_2O_t}$ is proportional to H_2O_t concentration works well (Zhang et al., 1991a; Nowak and Behrens, 1997). Hence, we first give the following expression of $D_{H_2O_t}$ at low H_2O_t:

$$D_{H_2O_t} = \frac{C}{C_0}\exp\left(10.49 - \frac{10{,}661}{T} - \frac{1.772P}{T}\right), \quad (12)$$

where T is in Kelvin, P is in megaPascal, $D_{H_2O_t}$ is in micrometer squared per second and C_0 equals 1% H_2O_t. The above expression is similar to that in Zhang (1999) but with an added term to account for the pressure effect.

In order to develop a more general equation to directly calculate $D_{H_2O_t}$ to high H_2O_t, we first examine the variation of $D_{H_2O_t}$ calculated from (Eqs. (2), (4), and (11) by assuming species equilibrium. It

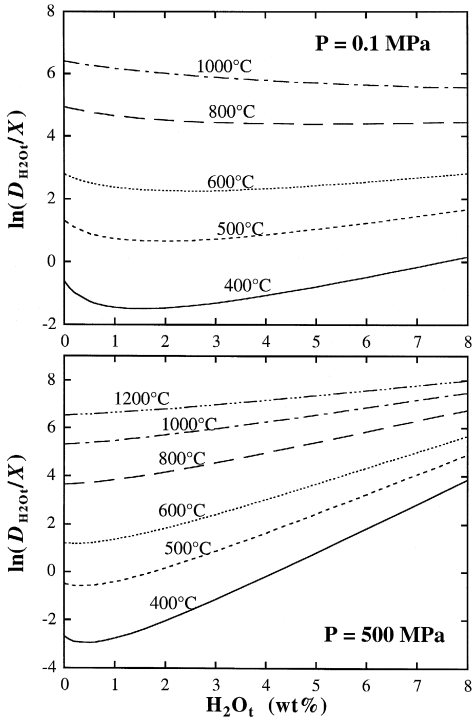

Fig. 8. The values of $\ln(D_{H_2O_t}/X)$ vs. H_2O_t at different temperatures and two pressures. $D_{H_2O_t}$ is in micrometer squared per second and X is the mole fraction of H_2O_t. The calculation assumes local species equilibration, and hence, caution should be exercised when applying the results to low-T diffusion (such as 400°C).

Table 4
Calculated $D_{H_2O_t}$ values at selected T, P, and H_2O_t
The $\log_{10} D_{H_2O_t}$ (in $\mu m^2/s$) values are calculated by combining (Eqs. (11), (2), and (4).

T (°C)	P (MPa)	$\log_{10} D_{H_2O_t}$ (in $\mu m^2/s$) at a given H_2O_t (wt.%)					
		0.1	0.5	1	2	4	6
400	0.1	−3.10	−2.60	−2.38	−2.09	1.62	1.19
600	0.1	−1.56	−0.95	−0.71	−0.46	−0.14	0.12
800	0.1	−0.61	0.03	0.28	0.51	0.76	0.93
1000	0.1	0.03	0.68	0.93	1.16	1.36	1.46
400	500	−3.97	−3.33	−2.95	−2.33	−1.23	−0.19
600	500	−2.23	−1.52	−1.15	−0.65	0.16	0.90
800	500	−1.16	−0.43	−0.08	0.36	1.00	1.56
1000	500	−0.43	0.29	0.63	1.03	1.56	1.99
1200	500	0.10	0.81	1.14	1.51	1.96	2.30

turns out that the variation can be described well by the empirical expression:

$$D_{H_2O_t} = X\exp(c_1)\left[1+\exp\left(c_2+c_3X+c_4\sqrt{X}\right)\right], \quad (13)$$

where c_1, c_2, c_3, and c_4 are four constant. In the above expression, the constant $\exp(c_1)$ is used (instead of simply c_1) to simplify later expressions. Fitting $D_{H_2O_t}$ values at different T and P, it is found that c_1, c_2, and c_3 are roughly linear to $1/T$ and P/T, $c_2 - c_1 = 56$; and c_4 is linear to $1/T^2$ and roughly independent of P. Accounting for these relations, the following expression is obtained by fitting the data to describe the dependence of $D_{H_2O_t}$ on T, P, and X:

$$D_{H_2O_t} = X\exp(m)\left\{1+\exp\left[56+m+X\left(-34.1+\frac{44{,}620}{T}+\frac{5[illegible]}{T}\right)-\sqrt{X}\left(0.091+\frac{4.77\times10^6}{T^2}\right)\right]\right\}, \quad (14)$$

where m is given by

$$m = -20.79-5030/T-1.4P/T. \quad (15)$$

This expression of $D_{H_2O_t}$ can reproduce $D_{H_2O_t}$ values calculated using (Eqs. (2), (4) and (4) to within 20%. Note that the above expressions (Eqs. 12 and 14) assume species equilibrium, and hence, caution should be exercised when applying it to low temperatures (such as 400°C).

4.4. Comparison with previous diffusion data

Our new results are consistent with previous results of various authors. Delaney and Karsten (1981) suggested an exponential dependence of $D_{H_2O_t}$ on H_2O_t in rhyolitic melts in the concentration range of 0.2–3.7%. Zhang et al. (1991a) found that at low H_2O_t ($\leq 1.8\%$), $D_{H_2O_t}$ is roughly linear to H_2O_t, and H_2O diffusion can be modeled assuming an H_2O_t-independent $D_{H_2O_m}$. Nowak and Behrens (1997) showed that the linear dependence of $D_{H_2O_m}$ on H_2O_t only holds up to 2% H_2O_t, and at greater H_2O_t, the dependence is exponential. As shown by Nowak and Behrens (1997), the rapid increase of $D_{H_2O_t}$ with H_2O_t at $H_2O_t > 3\%$ cannot be accounted for by an H_2O_t-independent $D_{H_2O_m}$. In this study, we obtained for the first time an expression that describes $D_{H_2O_t}$ as a function of H_2O_t at both low and high H_2O_t. This expression, assuming an exponential dependence of $D_{H_2O_m}$ on H_2O_t, is consistent

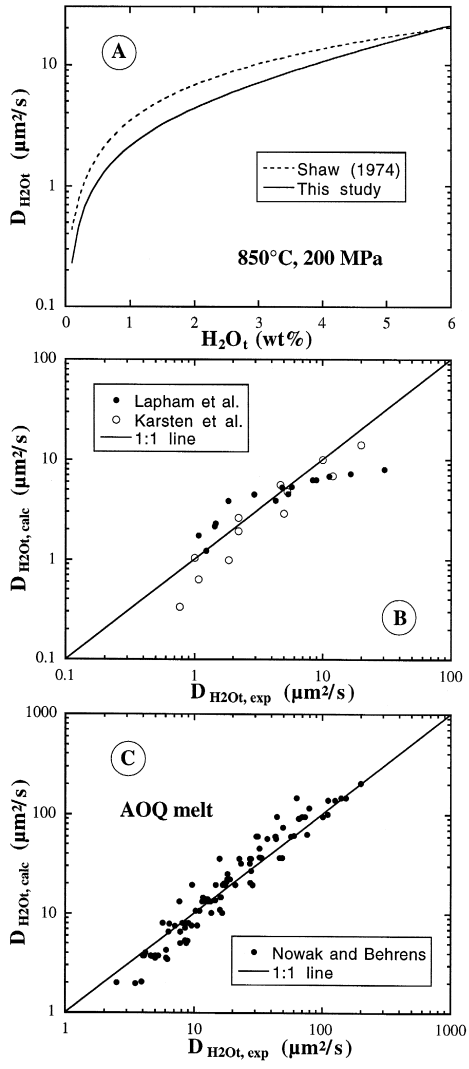

Fig. 9. Comparison of this study with previous data. None of these previous data is used in calibrating the diffusivity formulation of this study. The data of Lapham et al. (1984) cover $T-P$ space of 850°C and 50–70 MPa. The data of Karsten et al. (1982) cover 650–950°C and 70 MPa. The data of Nowak and Behrens (1997) cover 800–1200°C and 50–500 MPa.

with the results of Zhang et al. (1991a) as well as those of Nowak and Behrens (1997).

In Fig. 9, $D_{H_2O_t}$ values calculated from our formulation (combining (Eqs. 2, 4, and 11)) are compared to the results of Shaw (1974), Karsten et al. (1982), Lapham et al. (1984), and Nowak and Behrens (1997). Although none of these data is used as input for our formulation, all of these data can be calculated to within a factor of two, except for a few points which were obtained near the end of some diffusion-couple profiles using the Boltzmann–Matano technique and hence, have relatively large errors. Therefore, we conclude that all available H_2O diffusivity data for rhyolitic and haplogranitic melts are reconciled at both low and high H_2O_t, low and high temperature, and low and high pressure. Our formulation can hence be applied to calculate H_2O diffusion during bubble growth and volcanic eruptions. Nevertheless, there is still a need to improve the understanding of the pressure effect on H_2O diffusion.

It is worth noting that the dependence of $D_{H_2O_t}$ on H_2O_t is similar to that of viscosity on H_2O_t (Hess and Dingwell, 1996; Schulze et al., 1996) at least for $H_2O_t > 1\%$. However, the atomic mechanisms for the two transport processes are different, and diffusivities calculated from viscosity data using the Eyring equation are orders of magnitude different from $D_{H_2O_t}$ (Behrens and Nowak, 1997).

5. Conclusions

A comprehensive investigation of H_2O diffusion in rhyolitic melt has been carried out. Although there are still some analytical and experimental problems, including uncertainties in the calibration of the IR technique and H_2O loss from diffusion-couple experiments, we obtained good diffusion data in a wide range of T, P, and H_2O_t. One region without experimental diffusion data coverage owing to bubbling problem is at high H_2O_t and low P. Diffusion profiles covering a large range of H_2O_t are well-fit by assuming that molecular H_2O is the diffusing species (Zhang et al., 1991a) and that the diffusivity of molecular H_2O increases exponentially with H_2O_t. All diffusion data are quantified in this manner and the high degree of consistency in data extracted from both high and low H_2O_t experiments (Fig. 7) demonstrates that the assumptions capture the essence of H_2O diffusion. All available H_2O diffusion data are now reconciled. Our assessment is that the formulation for $D_{H_2O_t}$ can predict D to within a factor of two at 0–800 MPa (except at low P and high H_2O_t), and with better accuracy at 500 MPa. One can use the $D_{H_2O_t}$ values to model bubble growth in rhyolitic magmas although the pressure dependence of the diffusivities still needs some improvement.

Acknowledgements

We thank O. Navon and A. Proussevitch for careful and insightful reviews. This research is supported by German Christian Kuhlemann Foundation (Germany), German DAAD, and US NSF grant EAR-9972937.

References

Behrens, H., Nowak, M., 1997. The mechanisms of water diffusion in polymerized silicate melts. Contrib. Mineral. Petrol. 126, 377–385.

Behrens, H., Romano, C., Nowak, M., Holtz, F., Dingwell, D.B., 1996. Near-infrared spectroscopic determination of water species in glasses of the system $MAlSi_3O_8$ (M = LiNa, K): an interlaboratory study. Chem. Geol. 128, 41–63.

Cooper, R.F., Fanselow, J.B., Poker, D.B., 1996. The mechanism of oxidation of a basaltic glass: chemical diffusion of network-modifying cations. Geochim. Cosmochim. Acta 60, 3253–3265.

Delaney, J.R., Karsten, J.L., 1981. Ion microprobe studies of water in silicate melts: concentration-dependent water diffusion in obsidian. Earth Planet. Sci. Lett. 52, 192–202.

Doremus, R.H., 1995. Diffusion of water in silica glass. J. Mater. Res. 10, 2379–2389.

Friedman, I., Long, W., 1976. Hydration rate of obsidian. Science 191, 347–352.

Ganguly, J., Bhattacharya, R.N., Chakraborty, S., 1988. Convolution effect in the determination of compositional profiles and diffusion coefficients by microprobe step scans. Am. Mineral. 73, 901–909.

Hess, K., Dingwell, D.B., 1996. Viscosities of hydrous leucogranitic melts: a non-Arrhenian model. Am. Mineral. 81, 1297–1300.

Jambon, A., 1979. Diffusion of water in a granitic melt: an experimental study. Carnegie Inst. Washington, Year Book, 352–355.

Jambon, A., 1983. Diffusion dans les silicates fondus: un bilan des connaissances astuelles. Bull. Mineral. 106, 229–246.

Jambon, A., Zhang, Y., Stolper, E.M., 1992. Experimental dehydration of natural obsidian and estimation of D_{H_2O} at low water contents. Geochim. Cosmochim. Acta 56, 2931–2935.

Karsten, J.L., Holloway, J.R., Delaney, J.R., 1982. Ion microprobe studies of water in silicate melts: temperature-dependent water diffusion in obsidian. Earth Planet. Sci. Lett. 59, 420–428.

Kohn, S.C., Dupree, R., Smith, M.E., 1989. A multinuclear magnetic resonance study of the structure of hydrous albite glasses. Geochim. Cosmochim. Acta 53, 2925–2935.

Lapham, K.E., Holloway, J.R., Delaney, J.R., 1984. Diffusion of H_2O and D_2O in obsidian at elevated temperatures and pressures. J. Non-Cryst. Solids 67, 179–191.

Moulson, A.J., Roberts, J.P., 1961. Water in silica glass. Trans. Faraday Soc. 57, 1208–1216.

Mungall, J.E., Romano, C., Dingwell, D.B., 1998. Multicomponent diffusion in the molten system K_2O–Na_2O–Al_2O_3–SiO_2–H_2O. Am. Mineral. 83, 685–699.

Navon, O., Chekhmir, A., Lyakhovsky, V., 1998. Bubble growth in highly viscous melts: theory, experiments, and autoexplosivity of dome lavas. Earth Planet. Sci. Lett. 160, 763–776.

Nowak, M., Behrens, H., 1997. An experimental investigation on diffusion of water in haplogranitic melts. Contrib. Mineral. Petrol. 126, 365–376.

Proussevitch, A.A., Sahagian, D.L., 1998. Dynamics and energetics of bubble growth in magmas: analytical formulation and numerical modeling. J. Geophys. Res. 103, 18223–18251.

Schulze, F., Behrens, H., Holtz, F., Roux, J., Johannes, W., 1996. The influence of H_2O on the viscosity of a haplogranitic melt. Am. Mineral. 81, 1155–1165.

Shaw, H.R., 1974. Diffusion of H_2O in granitic liquids: I. Experimental data; II. Mass transfer in magma chambers. In: Hofmann, A.W., Giletti, B.J., Yoder, H.S., Yund, R.A. (Eds.), Geochemical Transport and Kinetics. Carnegie Inst. Washington Publ., Washington, DC, pp. 139–170.

Stolper, E., 1982. The speciation of water in silicate melts. Geochim. Cosmochim. Acta 46, 2609–2620.

Sykes, D., Kubicki, J.D., 1993. A model for H_2O solubility mechanisms in albite melts from infrared spectroscopy and molecular orbital calculations. Geochim. Cosmochim. Acta 57, 1039–1052.

Wang, L., Zhang, Y., Essene, E.J., 1996. Diffusion of the hydrous component in pyrope. Am. Mineral. 81, 706–718.

Wasserburg, G.J., 1988. Diffusion of water in silicate melts. J. Geol. 96, 363–367.

Watson, E.B., 1994. Diffusion in volatile-bearing magmas. Rev. Mineral. 30, 371–411.

Withers, A.C., Behrens, H., 1999. Temperature induced changes in the NIR spectra of hydrous albitic and rhyolitic glasses between 300 and 100 K. Phys. Chem. Miner. 27, 119–132.

Zhang, Y., 1999. H_2O in rhyolitic glasses and melts: measurement, speciation, solubility, and diffusion. Rev. Geophys. 37, 493–516.

Zhang, Y., Behrens, H., 1998. H_2O diffusion in silicate glasses and melts. Min. Mag. 62A, 1695–1696.

Zhang, Y., Belcher, R., Ihinger, P.D., Wang, L., Xu, Z., Newman, S., 1997. New calibration of infrared measurement of water in rhyolitic glasses. Geochim. Cosmochim. Acta 61, 3089–3100.

Zhang, Y., Stolper, E.M., 1991. Water diffusion in basaltic melts. Nature 351, 306–309.

Zhang, Y., Stolper, E.M., Ihinger, P.D., 1995. Kinetics of reaction $H_2O + O = 2OH$ in rhyolitic glasses: preliminary results. Am. Mineral. 80, 593–612.

Zhang, Y., Stolper, E.M., Wasserburg, G.J., 1991a. Diffusion of water in rhyolitic glasses. Geochim. Cosmochim. Acta 55, 441–456.

Zhang, Y., Stolper, E.M., Wasserburg, G.J., 1991b. Diffusion of a multi-species component and its role in the diffusion of water and oxygen in silicates. Earth Planet. Sci. Lett. 103, 228–240.